

Plasma Sci. Technol. **24** (2022) 085402 (7pp) https://doi.org/10.1088/2058-6272/ac6570

Argon plume transition from a hollow swell to a diffuse swell with increasing amplitude of a trapezoidal voltage

Junyu CHEN (陈俊宇)[1], **Furong ZHANG** (张芙蓉)[1], **Pengying JIA** (贾鹏英)[2], **Na ZHAO** (赵娜)[1,3], **Kaiyue WU** (吴凯玥)[2], **Jiacun WU** (武珈存)[1], **Junxia RAN** (冉俊霞)[1], **Xuexia PANG** (庞学霞)[1,2] **and Xuechen LI** (李雪辰)[1,2,*]

[1] College of Physics Science & Technology, Hebei University, Baoding 071002, People's Republic of China
[2] Institute of Life Science & Green Development, Hebei University, Baoding 071002, People's Republic of China
[3] School of Mathematics and Physics, Handan University, Handan 056005, People's Republic of China

E-mail: plasmalab@126.com and xuechenli@126.com

Received 26 October 2021, revised 3 April 2022
Accepted for publication 7 April 2022
Published 29 June 2022

Abstract

Atmospheric pressure plasma jets can generate a remote plasma plume, which usually presents a conical or cylindrical morphology. Despite a few morphologies being observed, efforts should be made to obtain more plume structures because streamer dynamics may be revealed from them. For this purpose, an argon plasma plume excited by a trapezoidal voltage is investigated, which presents two kinds of swells (a hollow swell and a diffuse swell) with increasing voltage amplitude (V_p). The results indicate that there are two positive discharges (D_{p1} and D_{p2}) and one negative discharge (D_n) per voltage cycle for both of the swells. With increasing V_p, the inception voltage and discharge intensity increase for every positive discharge, while they decrease for the negative discharge. Fast photography reveals that the positive streamer (D_{p2}) leaves different tracks in the two swells, which are curved in the hollow swell and randomly branched in the diffuse swell. The different tracks of D_{p2} are explained with the consideration of applied field strength and residual positive ions of D_{p1}. The existence of residual positive ions is finally verified from optical emission spectra.

Keywords: plasma jet, plume morphology, streamer behavior, optical emission spectra

(Some figures may appear in colour only in the online journal)

1. Introduction

A plasma jet can generate a remote plasma plume in open space rather than in a confined gap. Thus, it can be used for direct treatment and there is no limitation on the size of the object to be treated [1]. Given this advantage, a plasma jet has become a very attractive tool in various application fields, such as surface modification [2–4], biomedicine [5], water purification [6, 7], material growth [8], etching [9], and so on.

Although a plasma plume fed by inert gas looks continuous to the naked eye [10–13], it is essentially composed of discrete emission layers (also referred to as a plasma bullet) [14], which propagates at a velocity in the order of 10^3–10^5 m s^{-1} [10, 14–16]. The fast plasma bullet originates from positive or negative streamers propagating along the working-gas stream [11, 13, 17]. The head of a streamer is a highly effective chemical reactor that can produce active species for diversified applications [16, 18, 19]. The time-integrated track of streamers is the emission profile (morphology) of a plasma plume, which is one of the major characteristics of a plasma jet [20]. Under most circumstances, streamers propagate repeatedly along the stream axis [10, 21], leading to a cylindrical plume [14]. Due to the inclusion of diffused air, the diameter of repeated streamers decreases with increasing propagation distance, resulting in a solid plume with a conical shape [10]. The repeatability of streamers

* Author to whom any correspondence should be addressed.

deteriorates with seed electrons left by the previous discharge less than 10^9 cm^{-3} [22, 23]. That is to say, the solid cone may vary its morphology with decreasing driving frequency. In fact, the solid cone transited to a hollow cone, which originated from the propagation of branched streamers in the interfacial layer between the argon stream and the ambient air [11]. At the tail of a conical plume, a fork-like structure was created since streamers tended to follow the neon channel, which was branched by turbulence at plume tail [24]. Besides, a feather-like plume was witnessed with argon or helium used as working gas [25, 26], which was attributed to dim streamers surrounding the central bright streamer due to Penning ionization.

A striated plume was observed inside the tube of a pulsed argon plasma jet [27]. Outside the tube, a striated plume was formed with helium or neon used as working gas [28–30]. Droplet striations, also referred to as multiple swells, were formed in an argon or neon plume [31, 32], which were attributed to the turbulence of the working gas [33]. Multiple swells were formed under a laminar flow [34], which resulted from the periodical diameter variation of propagating streamers due to discharge enhancement by active species. Besides multiple swells, a single swell was produced near the jet nozzle [35], which resulted from the distinct dynamic behaviors of different streamers in one voltage pulse. All in all, streamer dynamics can be revealed through exploring the formation mechanism of plume morphologies. Despite a few morphologies being observed, efforts should be made to obtain more plume structures.

In this work, two kinds of single swells, namely a hollow swell and a diffuse swell, are generated at the argon plume tail excited by a trapezoidal voltage. Using fast photography, distinct streamer dynamics are revealed for the two kinds of swells.

2. Experiment setup

Figure 1 presents a schematic diagram of the experimental setup. The single-electrode jet is composed of a tungsten rod (6.0 cm in length, 1.0 mm in diameter, and 0.5 mm in tip radius), which is centered in a glass tube (inner and outer diameters of 5.0 mm and 8.0 mm, respectively). The rod tip is aligned with the nozzle of the jet, which is fed with argon (99.999% purity) after being regulated by a mass flow controller (Sevenstar CS200A). Plume images are captured by a digital camera (Canon EOS 5D Mark IV) with different exposure time (t_{exp}). Applied voltage to the jet is detected by a high voltage probe (Tektronix P6015A), which is defined as real voltage (as will be mentioned later). Electric current in the circuit is measured by a coil (Pearson 8600). Waveforms of real voltage and electric current are simultaneously recorded by an oscilloscope (Tektronix DPO4104). Mounted with an intensified charge-coupled devices (ICCD, PI MAX4), a spectrometer (ACTON SP2750) with a grating of 2400 grooves per mm is utilized to collect spatially resolved spectrum through the varying detection position of a fiber. A signal generator (Tektronix AFG 3052C) produces two

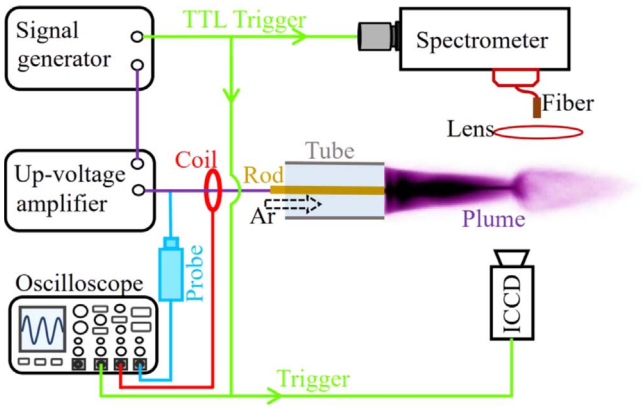

Figure 1. Schematic diagram of the experimental setup.

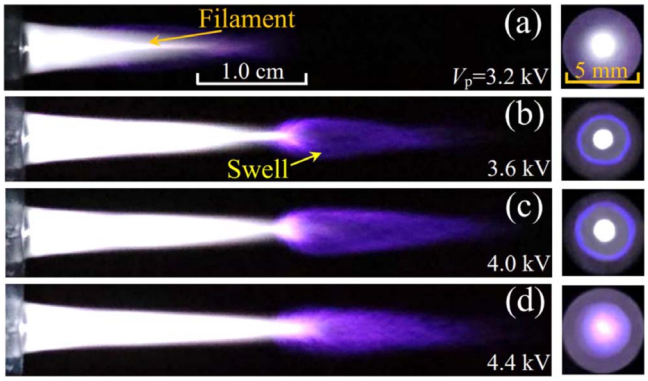

Figure 2. Side-view (left) and end-view (right) images with varying V_p of 3.2 kV (a), 3.6 kV (b), 4.0 kV (c), and 4.4 kV (d). The end-view images are focused on the middle of the swell. Q is 2.0 l min^{-1}, and t_{exp} is 0.1 s.

synchronized 6.0 kHz signals, one of which is a trapezoidal wave used to excite the jet after 2000 times amplification by an up-voltage amplifier (TREK 20/20). The other is a transistor transistor logic (TTL) signal to trigger two independent ICCDs. One ICCD (Andor DH334T) is used to take discharge images and the other ICCD (PI MAX4) is utilized to collect spectrum with short t_{exp}. Moreover, the TTL signal is displayed by the oscilloscope along with the current waveform. By subtracting the time lag between the TTL and the electric current, the ICCD can be synchronized with the discharge. Temporally resolved images or spectrum can then be obtained by varying gate moment of the ICCD.

3. Results and discussion

As presented in figure 2, a diffuse plume with a central filament, similar to that reported previously [12], is firstly generated downstream of the jet nozzle with increasing amplitude of the trapezoidal voltage (V_p). Due to the ingredient of diffused air [10], the plume (3.2 kV) is conical, which elongates along the argon stream with increasing V_p. When V_p reaches 3.6 kV, a purple hollow swell is formed near the plume tail. The hollow structure is clear in the end-view image, where a dim void exists between the purple ring and the central spot.

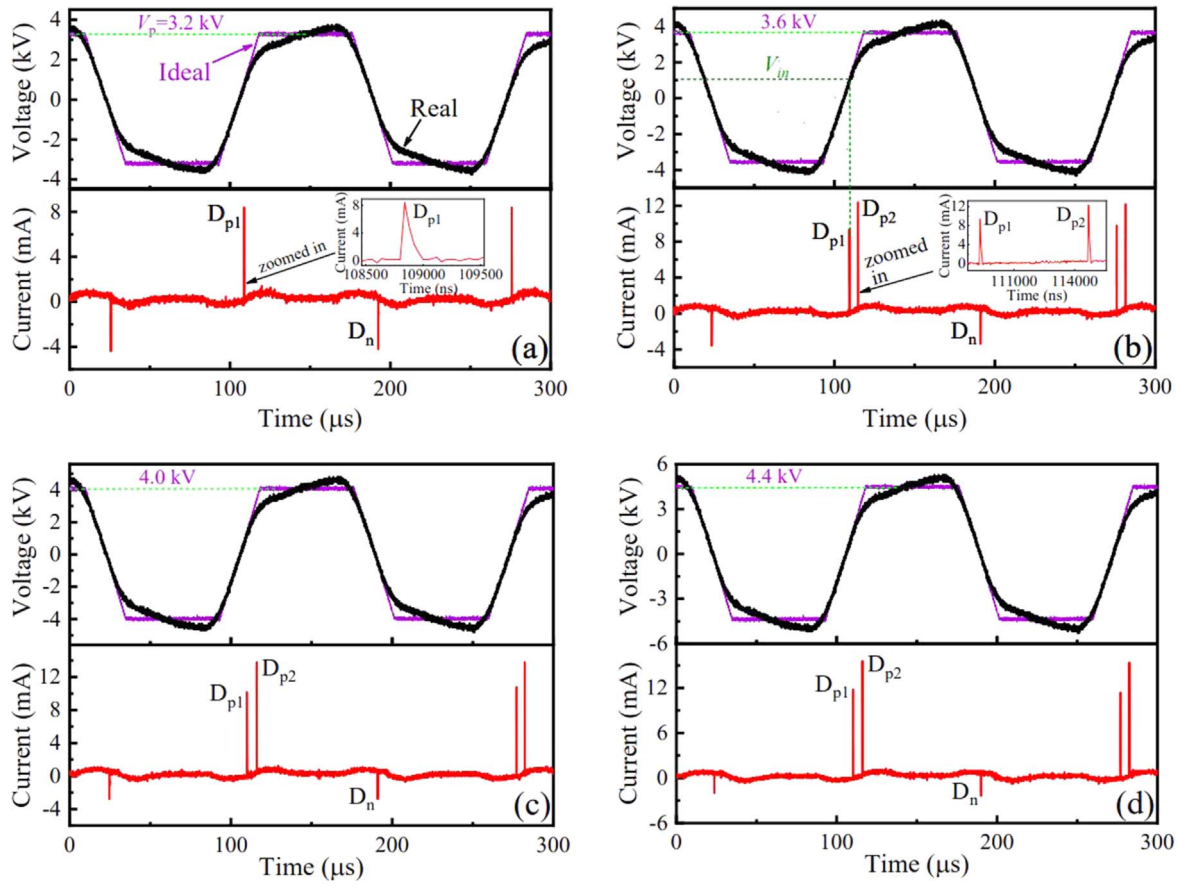

Figure 3. Waveforms of voltage and current. (a)–(d) Corresponding to figures 2(a)–(d), respectively.

The hollow swell slightly grows with increasing V_p (4.0 kV). The hollow structure disappears and a diffuse swell is formed when V_p surpasses about 4.4 kV. Hence, two kinds of single swells including the hollow swell and the diffuse swell have been observed at the plume tail.

During the morphology evolution with varying V_p, waveforms of voltage and electric current are recorded, as illustrated in figure 3. Here, the ideal voltage is obtained through multiplying the output of the signal generator by 2000, whose amplitude is the aforementioned V_p. In addition, electric current (discharge current) in figure 3 is obtained from total current by subtracting displacement current, which is directly measured in the circuit when discharge does not initiate without argon flow. Due to the restriction of the amplifier, there is distortion between ideal voltage and real voltage. For this reason, it is impossible to generate a real triangle wave because the triangle apex will be clipped to make it more like a trapezoidal wave. Even though a plume with a well can also be excited by a sinusoidal voltage, there are too many discharge pulses (at least 5 pulses) per voltage cycle, which increases the difficulty in revealing the plume dynamics. Hence, a tailored trapezoidal voltage is used to drive the plasma jet. Obviously, real voltage amplitude increases with increasing V_p. It can be seen in figure 3(a) that there is one positive discharge (D_{p1}) and one negative discharge (D_n) per voltage cycle for the diffuse plume. Besides, D_{p1} has a higher intensity than D_n. As indicated in the enlarged current in figure 3(b), the pulse duration is 160 ns for D_{p1}, 200 ns for D_{p2}, and 240 ns for D_n. The time interval between D_{p1} and D_{p2} is about 5.36 μs. For the hollow swell (figures 3(b) and (c)) or the diffuse swell (figure 3(d)), there are two positive discharges (D_{p1} and D_{p2}) and one D_n per voltage cycle. Among these discharge pulses, D_{p2} has the highest intensity. In other words, the number of positive discharges is mainly influenced by V_p, which is one under a low V_p and two with a high V_p.

From figure 3, it can also be found that inception voltage (V_{in}, absolute value of real voltage when one discharge initiates) and discharge intensity of every discharge change with increasing V_p. V_{in} was used to describe partial discharge (also referred to as a dielectric barrier discharge), which is the value of applied voltage when the first discharge initiates during one half cycle. Here, the concept of V_{in} is used in the discharge of the plasma jet [12, 36]. For example, V_{in} of D_{p1} means the voltage value when D_{p1} just initiates. Inception voltages and discharge intensities as functions of V_p have been investigated, as illustrated in figure 4. It is found that V_{in} increases for D_{p1} and D_{p2}, while decreases for D_n with increasing V_p. Similarly, discharge intensity increases for D_{p1} and D_{p2}, while it decreases for D_n with increasing V_p.

As is well known, streamer regime is involved in plume discharge [12, 13, 37]. Therefore, D_{p1} and D_{p2} are positive streamers, while D_n is a negative streamer. The tracks of these streamers are captured by the ICCD, as presented in figure 5.

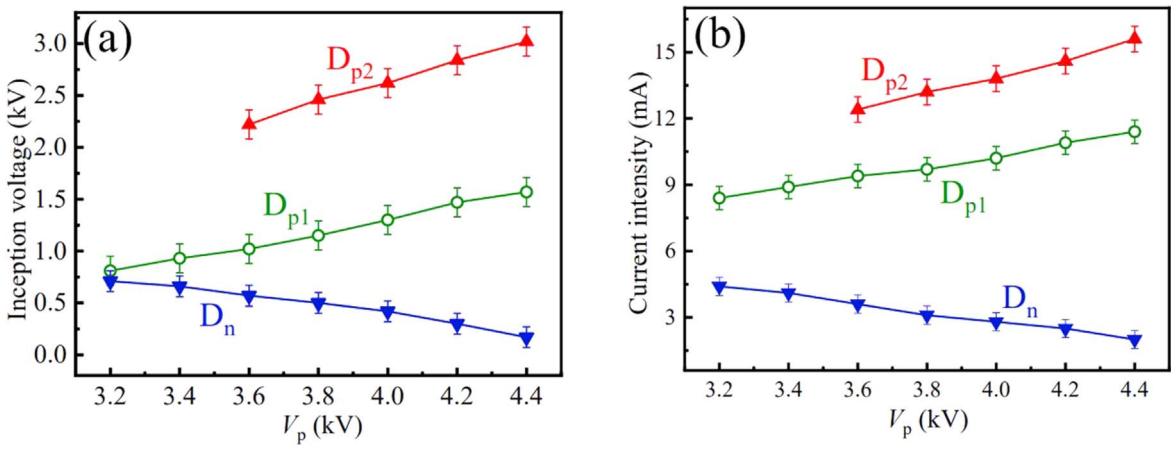

Figure 4. Inception voltage (a) and current intensity (b) of every discharge pulse as functions of V_p. Q is 2.0 l min^{-1}.

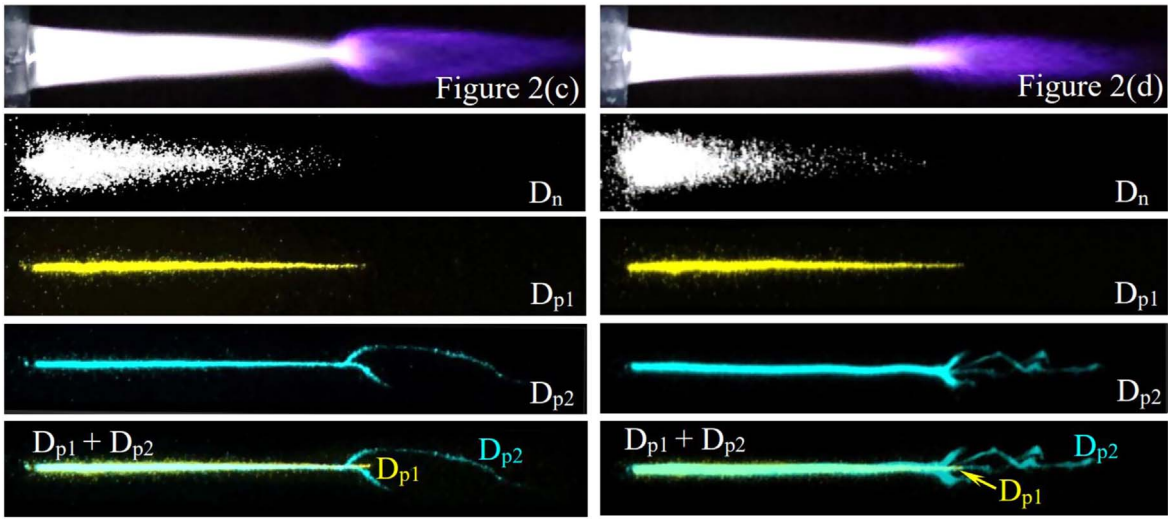

Figure 5. Single-shot ICCD images exposed to D_n, D_{p1}, and D_{p2} for the hollow swell (figure 2(c)) (the left) and the diffuse swell (figure 2(d)) (the right). The bottom image is the superposition of the two false-color images exposed to D_{p1} and D_{p2}.c.

For the hollow swell or the diffuse swell, the negative streamer (D_n) leaves a conical plump track, while the positive streamers (D_{p1} and D_{p2}) leave filamentary tracks. In contrast to D_{p1}, D_{p2} can propagate a longer distance. Interestingly, D_{p2} repeats the track of D_{p1} and leaves a straight line in the left part. In the right part, D_{p2} tends to detour the tail of D_{p1}, leaving a curved track that constitutes the hollow swell. However, D_{p2} tends to cross the tail of D_{p1}, leaving random branches in the diffuse swell. Accordingly, the distinct morphologies of the hollow swell and the diffuse swell originate from the different propagating behaviors of the positive streamer (D_{p2}).

Figure 6(a) presents optical emission spectrum scanned from 300 to 800 nm for the hollow swell (a similar spectrum for the diffuse well, hence not shown here). Spectral lines of Ar I (4p → 4s transitions) are dominant in the long wavelength range. Besides Ar I, the second positive system of N_2 ($C^3\Pi_u$–$B^3\Pi_g$) and OH ($A^2\sum^+$–$X^2\Pi$) can also be discerned [38]. The intensity ratio of spectral lines (763.7 to 772.6 nm) is positively related to electron temperature, which is determined by electric field strength [39, 40]. Based on spatiotemporally resolved spectrum, spatial distribution of line intensity ratio (representing field strength) is obtained for D_{p2}, as plotted in figure 6(b). It can be found that there is a minimal field strength during the propagation of the positive streamer (D_{p2}) for both of the swells. In contrast to the hollow plume, the diffuse plume possesses higher maximal field strength during D_{p2}.

As is well known, charge separation between electrons and positive ions is a prerequisite for a streamer propagation [10]. The applied field is reinforced by the induced field of separated charges. In a positive streamer, electrons drift towards and enter the needle anode [12, 13, 34], leading to the positive current in figure 3. Along with the entering electrons on the anode, the track of the positive streamer is positively charged by residual positive ions, which have been confirmed by numerical simulations [41–43]. Although positive ions are considered to be stationary for a positive discharge, this is not the case for a negative discharge, especially near the needle cathode, where positive ions can be accelerated to a high

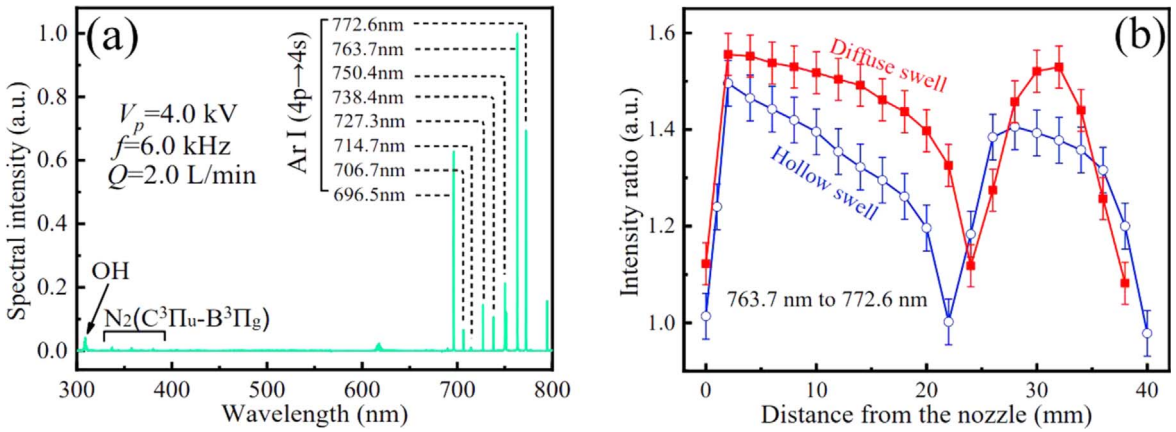

Figure 6. (a) Optical emission spectrum scanned from 300 to 800 nm for the plasma plume (figure 2(c)). (b) Intensity ratio of D_{p2} as a function of distance for the hollow swell (figure 2(c)) and the diffuse one (figure 2(d)).

velocity. Through ions bombarding, secondary electrons are produced from the cathode [44], resulting in the negative current in figure 3. It is reasonable to speculate that the track of a negative streamer is negatively charged accompanying the bombarding positive ions and the emitted electrons on the cathode. Before the subsequent discharge, residual electrons in the track can be neglected because of their high mobility. However, electrons can be attached by electronegative species, such as O_2, OH, NO, NO_2, O, etc to form negative charges [45–49]. Compared with electrons, these negative charges have a lower mobility. Hence, a negative streamer can provide the forthcoming streamer with residual negative charges.

Residual negative charges of D_n diminish with increasing V_p, which can be found from the weakening D_n with V_p (figure 4). Residual negative charges of D_n can lower the field threshold for breakdown of the forthcoming discharge (D_{p1}) through releasing seed electrons [50, 51]. Less residual negative charges mean that a higher applied field is needed to initiate D_{p1}, leading to the rising V_{in} of D_{p1} with increasing V_p. As to the increasing intensity of D_{p1} with increasing V_p, the following two reasons can be considered. Firstly, applied field strength increases with increasing V_p, as mentioned above. A stronger discharge tends to initiate under a higher applied field [52]. Therefore, intensity of D_{p1} increases with increasing V_p. Secondly, because the streamer head of D_{p1} is positively charged [10, 53], residual negative charges can partly counteract or neutralize the charges in the streamer head, which results in the reduction of the induced field. Hence, less residual negative charges mean a higher induced field of D_{p1} with increasing V_p. That is to say, net field strength of D_{p1} increases with increasing V_p. As a result, intensity of D_{p1} increases with increasing V_p because discharge intensity of a streamer is determined by net field strength [42].

As a positive streamer, D_{p1} leaves a positively-charged track [40, 41], where residual positive charges become denser with increasing V_p due to the increasing discharge intensity. The denser residual positive charges produce a higher field opposing the initiation of D_{p2}. Thus, a higher voltage is needed to initiate D_{p2} with increasing V_p. Therefore, V_{in} of D_{p2} increases with V_p. During the propagation of the positive streamer (D_{p2}), positive charges left by D_{p1} can enhance those of the positive streamer head, leading to a higher induced field. Apparently, the induced field increases when residual positive charges get denser with increasing V_p. In combination with the increasing V_{in}, it can be inferred that net field strength increases with increasing V_p. Hence, discharge intensity of D_{p2} increases with V_p.

The stronger D_{p2} provides the forthcoming discharge (D_n) with denser residual positive charges, which produce a higher electric field to help the initiation of D_n after voltage polarity is reversed. Hence, a lower voltage is needed to initiate D_n as V_p increases. Consequently, V_{in} of D_n decreases with increasing V_p. Besides, negative charges in the negative streamer head can be partly counteracted by residual positive charges of D_{p2}. Hence, less negative charges are presented in the streamer head of D_n with increasing V_p, which induce a weaker field, leading to the decreasing intensity of D_n with increasing V_p.

As mentioned before, D_{p2} has a curved track in the hollow swell. In fact, the curved track was found for a streamer propagating in a tube [54, 55], which was attributed to a turbulent flow [54]. However, our gas flow is 2.0 l min^{-1}, corresponding to a Reynolds number of 607, which is much lower than that of a turbulent flow [33]. Hence, turbulent flow is not the cause for the curved track. The underlying physics of the curved track of D_{p2} is similar to the snake-like propagation of streamers in a meandering plume [56]. In the following, the curved track will be explained from the influence of residual positive charges, which are left in the track of positive streamers [40, 41]. In fact, residual positive charges are not uniformly distributed in the track, and a large number of them are left at the streamer end where the positive streamer head stops propagating when no more secondary electron avalanches are induced to neutralize the positive streamer head [53]. Take D_{p1} for example, one can deduce that there is a cloud of residual positive ions at the streamer end of D_{p1}. Due to low mobility of positive ions [57], the cloud of residual positive charges at the streamer end of D_{p1}

can be thought as standing still, which will then influence the propagating behavior of D_{p2}.

Electric field strength is reduced by the cloud of residual positive charges when the positive streamer (D_{p2}) is approaching. Maximal field strength will present at the periphery of the cloud, as pointed out by numerical simulations [43, 58]. Hence, secondary electron avalanches tend to initiate at the locations with maximal field strength [45], and D_{p2} will be deflected toward the periphery, leading to a curved propagation. When D_{p2} propagates away from the cloud of residual positive charges, maximal field strength will appear in the stream center leading to the backward deflection of D_{p2} [43, 58]. Hence, a curved track is left by D_{p2} due to its detouring the cloud of residual positive charges left by D_{p1}.

When the applied field is strong enough (the case of the diffuse swell), field threshold for breakdown can be satisfied in the region near the cloud of residual positive charges even though electric field is reduced by the cloud. In this case, secondary electron avalanches can be induced near the cloud. Hence, the positive streamer (D_{p2}) crosses the cloud, which is similar to the crossing behavior of surface streamers [40]. After crossing the ion cloud (at the right part of the ion cloud), a field is induced by the ion cloud, which is in the same direction as the applied field. Therefore, the electric field is greatly enhanced in the right part of the cloud, so that the field threshold for breakdown can be satisfied in lots of locations after crossing. Resultantly, secondary electron avalanches develop from different locations simultaneously, leading to the random branches of D_{p2}. This phenomenon is similar to the simulated and experimental results which account for the branching behavior of streamers under a high field [59, 60].

As analyzed above, residual positive charges of D_{p1} can reduce electric field strength when D_{p2} propagates in their left side. However, field strength is enhanced by them when D_{p2} propagates in their right side. Hence, a minimal field strength of D_{p2} appears near the cloud of residual positive charges of D_{p1}, which is in accordance with the result shown in figure 6(b).

4. Conclusions

In summary, using a trapezoidal wave, two types of single swells, including the hollow swell and the diffuse swell, are generated downstream of a single-electrode argon plasma jet, which present a transition from the hollow swell to the diffuse swell with increasing V_p. Results show that for both of the two kinds of swells, there are two positive discharges and one negative discharge per voltage cycle. With increasing V_p, inception voltage and discharge intensity increase for the positive discharges, while they decrease for the negative discharge. Fast photography reveals that the negative discharge is relatively diffuse and plump, and the positive discharges are filamentary. In addition, the hollow swell comes from the curved propagation of D_{p2}. In contrast, the diffuse swell results from the branched propagation of D_{p2}. The different behaviors of D_{p2} are analyzed after considering residual positive charges of D_{p1}. From optical emission spectrum, spatial distribution of electric field is obtained during the propagation of D_{p2}. There is a minimal field strength during D_{p2} propagation, which confirms the existence of residual positive charges of D_{p1}. Besides, inception voltage and discharge intensity as functions of V_p have also been qualitatively explained based on residual charges left in the track of the previous discharge.

Acknowledgments

This work is supported by National Natural Science Foundation of China (Nos. 51977057 and 11875121), the Natural Science Foundation of Hebei Province, China (Nos. A2020201025 and A2019201100), the Natural Science Interdisciplinary Research Program of Hebei University (Nos. DXK201908 and DXK202011), Post-graduate's Innovation Fund Project of Hebei Province (Nos. CXZZBS2019023 and CXZZBS2019029), and Post-graduate's Innovation Fund Project of Hebei University (Nos. HBU2021ss063 and HBU2021bs011).

References

[1] Lu X *et al* 2008 *Appl. Phys. Lett.* **92** 151504
[2] Engelhardt M *et al* 2017 *J. Phys. D: Appl. Phys.* **50** 015206
[3] Wu J *et al* 2021 *Plasma Sci. Technol.* **23** 085504
[4] Li X *et al* 2019 *Phys. Plasmas* **26** 023510
[5] Jiang C *et al* 2020 *Phys. Plasmas* **27** 113513
[6] Xu H *et al* 2017 *J. Phys. D: Appl. Phys.* **50** 245201
[7] Wu J *et al* 2020 *Plasma Sci. Technol.* **22** 055505
[8] Gozutok M *et al* 2016 *J. Phys. D: Appl. Phys.* **49** 474002
[9] Knoll A J *et al* 2018 *Plasma Process. Polym.* **15** 1700217
[10] Lu X *et al* 2014 *Phys. Rep.* **540** 123
[11] Li X *et al* 2018 *Plasma Process. Polym.* **15** 1700224
[12] Li X *et al* 2020 *Plasma Sources Sci. Technol.* **29** 065015
[13] Lu X and Laroussi M 2006 *J. Appl. Phys.* **100** 063302
[14] Teschke M *et al* 2005 *IEEE Trans. Plasma Sci.* **33** 310
[15] Maletić D *et al* 2017 *J. Phys. D: Appl. Phys.* **50** 145202
[16] Lu X *et al* 2016 *Phys. Rep.* **630** 1
[17] Laroussi M, Lu X and Keidar M 2017 *J. Appl. Phys.* **122** 020901
[18] Pinchuk M E *et al* 2020 *Appl. Phys. Lett.* **116** 164102
[19] Babaeva N Y and Naidis G V 2018 *Trends Biotechnol.* **36** 603
[20] Yamada H *et al* 2018 *Plasma Sources Sci. Technol.* **27** 05LT02
[21] Teodorescu M *et al* 2015 *Plasma Sources Sci. Technol.* **24** 025033
[22] Lu X and Ostrikov K 2018 *Appl. Phys. Rev.* **5** 031102
[23] Wu S and Lu X 2014 *Phys. Plasmas* **21** 123509
[24] Abdelaziz A A and Kim H H 2021 *Plasma Process. Polym.* **18** 2000190
[25] Colombo V *et al* 2014 *Plasma Process. Polym.* **11** 247
[26] Xian Y *et al* 2013 *Appl. Phys. Lett.* **103** 094103
[27] Kim S J, Chung T H and Bae S H 2010 *Phys. Plasmas* **17** 053504
[28] Seo Y S *et al* 2011 *Thin Solid Films* **519** 7071
[29] Yamada H *et al* 2020 *Phys. Plasmas* **27** 022107
[30] Fujiwara Y *et al* 2016 *Jpn. J. Appl. Phys.* **55** 010301
[31] Kang S K *et al* 2011 *IEEE Trans. Plasma Sci.* **39** 2318
[32] Darny T *et al* 2014 *IEEE Trans. Plasma Sci.* **42** 2504
[33] Wang R *et al* 2017 *Phys. Plasmas* **24** 093507
[34] Li X *et al* 2019 *Plasma Sources Sci. Technol.* **28** 055006

[35] Xian Y *et al* 2012 *Plasma Sources Sci. Technol.* **21** 034013
[36] Wu K *et al* 2020 *Phys. Plasmas* **27** 082308
[37] Lu X, Laroussi M and Puech V 2012 *Plasma Sources Sci. Technol.* **21** 034005
[38] Thiyagarajan M, Sarani A and Nicula C 2013 *J. Appl. Phys.* **113** 233302
[39] Zhang B *et al* 2014 *J. Appl. Phys.* **115** 043302
[40] Wu K *et al* 2019 *Plasma Process. Polym.* **16** 1900073
[41] Morrow R and Blackburn T R 2002 *J. Phys. D: Appl. Phys.* **35** 3199
[42] Babaeva N Y and Naidis G V 1996 *J. Phys. D: Appl. Phys.* **29** 2423
[43] Babaeva N Y and Naidis G V 2018 *Plasma Sources Sci. Technol.* **27** 075018
[44] Raizer Y P 1991 *Gas Discharge Physics* (Berlin: Springer)
[45] Jia P *et al* 2021 *Plasma Sources Sci. Technol.* **30** 095021
[46] Wu K *et al* 2022 *Plasma Sci. Technol.* **24** 055405
[47] Li X *et al* 2020 *Plasma Process. Polym.* **17** 1900223
[48] Gao K *et al* 2019 *AIP Adv.* **9** 115210
[49] McKay K *et al* 2013 *J. Phys. D: Appl. Phys.* **46** 464018
[50] Nie L *et al* 2016 *Phys. Plasmas* **23** 093518
[51] Chang L *et al* 2016 *Phys. Plasmas* **23** 123513
[52] Viegas P *et al* 2020 *Plasma Sources Sci. Technol.* **29** 095011
[53] Nijdam S *et al* 2020 *Plasma Sources Sci. Technol.* **29** 103001
[54] Wu S *et al* 2013 *Phys. Plasmas* **20** 023503
[55] Xia G *et al* 2015 *IEEE Trans. Plasma Sci.* **43** 1825
[56] Wu J *et al* 2021 *Phys. Plasmas* **28** 073501
[57] Chicheportiche A *et al* 2014 *J. Chem. Phys.* **141** 134302
[58] Li X *et al* 2022 *Phys. Fluids* **34** 027112
[59] Yuan X *et al* 2020 *J. Phys. D: Appl. Phys.* **53** 425204
[60] Hofmann S, Sobota A and Bruggeman P 2012 *IEEE Trans. Plasma Sci.* **40** 2888